Acta Crystallographica Section B
Structural Science
ISSN 0108-7681

Accurate molecular structures of chlorothiazide and hydrochlorothiazide by joint refinement against powder neutron and X-ray diffraction data

Charlotte K. Leech, Francesca P. A. Fabbiani,* Kenneth Shankland, William I. F. David and Richard M. Ibberson

ISIS Facility, STFC, Rutherford Appleton Laboratory, Chilton OX11 0QX, England

Correspondence e-mail: f.p.a.fabbiani@rl.ac.uk

Received 24 August 2007
Accepted 7 November 2007

The compounds chlorothiazide and hydrochlorothiazide (crystalline form II) have been studied in their fully hydrogenous forms by powder neutron diffraction on the GEM diffractometer. The results of joint Rietveld refinement of the structures against multi-bank neutron and single-bank X-ray powder data are reported and show that accurate and precise structural information can be obtained from polycrystalline molecular organic materials by this route.

1. Introduction

Chlorothiazide (CTZ, I), 6-chloro-4*H*-1,2,4-benzothiadiazine-7-sulfonamide 1,1-dioxide and hydrochlorothiazide (HCT, II), 6-chloro-2*H*-1,2,4-benzothiadiazine-7-sulfonamide 1,1-dioxide, are diuretic agents widely used in the clinical treatment of a number of disorders (see Fig. 1 for molecular structures).

Whilst preliminary X-ray crystallographic studies on CTZ were performed by Dupont & Dideberg (1970), its crystal structure was first solved from synchrotron powder data by Shankland *et al.* (1997). The single-crystal X-ray structure of HCT form I was first reported by Dupont & Dideberg (1972), whilst the structure of form II was solved from powder X-ray diffraction (PXRD) data (Florence, Johnston, Fernandes *et al.*, 2005).

These (and other) thiazides have been the subject of an extensive polymorph screen that has yielded new structures [*e.g.* (*S*)-trichlormethiazide; Fernandes *et al.*, 2007], new polymorphs (*e.g.* HCT form II, Florence, Johnston, Fernandes *et al.*, 2005) and a large number of solvated forms (*e.g.* CTZ DMSO, Johnston *et al.*, 2007*a*; CTZ *N*,*N*-DMA disolvate, Johnston *et al.*, 2007*b*; HCT-methyl acetate, Florence, Johnston & Shankland, 2005). Structures have been solved and refined primarily using single-crystal X-ray data, although several structures (including HCT form II and HCT-methyl-acetate) have been solved and refined using PXRD data alone. The experimental screen has been complemented by a crystal structure prediction (CSP) screen (see Johnston, Florence, Shankland *et al.*, 2007, for a full description of the methodologies involved) and of particular interest to the CSP element of the study is the determination of accurate H-atom positions, especially where the atoms in question are involved in hydrogen bonding (Cruz Cabeza *et al.*, 2006). Whilst, with modern single-crystal X-ray instrumentation H atoms can generally be located directly from Fourier maps (even when such atoms are disordered – see, for example, Parkin *et al.*, 2007), single-crystal neutron diffraction remains the method of choice for accurately pinpointing H-atom positions. This is a consequence of the fact that neutrons probe nuclear positions

Table 1
Examples of hydrogenous materials studied by powder neutron diffraction and complementary diffraction techniques.

PND = powder neutron diffraction; PXRD = powder X-ray diffraction; SXRD = single-crystal X-ray.

Compound	%H by No. of atoms	Data for refinement	Reference
$Cs_2C_2O_4{\cdot}H_2O$	18	SXRD + PND	Weller *et al.* (2007)
$[Re_4(\mu_3\text{-}H)_4(CO)_{12}]{\cdot}2C_6D_6$	7	SXRD + PND	Masciocchi *et al.* (1997)
$SO_2(NH_2)_2$ (sulfamide)	44	PND	Ibberson (1996)
$C_8H_{15}N_7O_2S_3$ (famotidine form B)	43	PXRD + PND	David *et al.* (2004)

directly, as opposed to implying them from electron-density maps. Furthermore, the lack of form-factor fall-off for neutrons helps in obtaining particularly high-resolution ($\sin\theta/\lambda$) diffraction data. Of course, not all compounds can be obtained as single crystals and whilst, as mentioned earlier, structure determination from PXRD data is now feasible routinely, powder neutron diffraction (PND) of hydrogenous organic materials is currently far from routine. This is a consequence of the large incoherent cross-section of the H atom which leads to a large degree of background scattering against which the coherent diffraction signal is hard to detect. This incoherent contribution can be largely eliminated by deuteration of the material under study, but it is often impractical or prohibitively expensive to fully deuterate a sample, and it may not be possible to obtain the deuterated material in the required crystalline form. Unsurprisingly, therefore, there have been relatively few examples of hydrogenous materials studied by PND; some are given in Table 1.

The last example in Table 1 is particularly impressive as its H-atom content and cell size are typical of a large number of molecular organic materials. Crucial to its successful refinement was the use of the GEM diffractometer at ISIS, which at 17*m* from the methane moderator has both high count-rate and good resolution. This, coupled with the large solid angle subtended by the detector banks, allows the coherent diffraction signal to be detected against the incoherent background.

The work presented here reports on the evolution and application of joint refinement against powder neutron and X-ray diffraction data for two organic molecules in their hydrogenated forms, with relatively high H-atom contents of 26 atom % (CTZ) and 32 atom % (HCT).

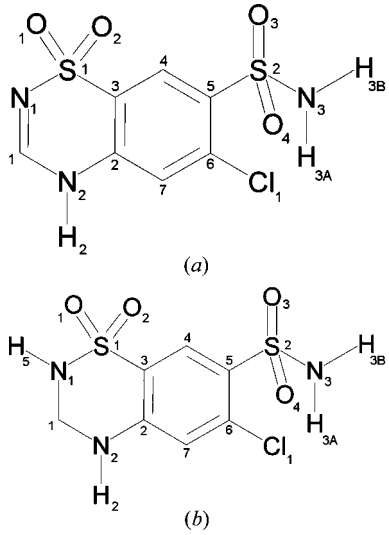

Figure 1
Molecular structures of (*a*) CTZ and (*b*) HCT, with associated numbering schemes.

2. Experimental

2.1. Crystallization procedure[1]

The title compounds were obtained from Sigma Aldrich. CTZ was used as received; HCT was prepared in form II following the method outlined in Florence, Johnston, Fernandes *et al.* (2005).

2.2. Data collection and processing

PND data were collected on the GEM diffractometer at the ISIS facility of the STFC Rutherford Appleton Laboratory. Samples were placed inside 5 mm vanadium cans and the sample height was 40 mm. CTZ data were collected at 130 K for $\sim$ 7.5 h, whilst HCT data were collected at 295 K for $\sim$ 12.5 h. All six detector banks were employed, covering a time-of-flight range of 379–20 000 µs. Data were normalized to the incident-beam monitor profile and corrected for detector efficiency effects using a previously recorded vanadium spectrum.

PXRD data for CTZ had been collected previously at 130 K on station 9.1 at the Daresbury Synchrotron Radiation Source, England (Shankland *et al.*, 1997). PXRD data for HCT were collected at 295 K on a Bruker AXS D8 diffractometer. The sample was loaded into a 0.7 mm borosilicate glass capillary and rotated throughout the data collection to minimize preferred orientation effects. Data were collected using a variable-count time (VCT) scheme in which the step time is increased with 2θ (Shankland *et al.*, 1997; Hill & Madsen, 2002).

2.3. Structure refinement

Refinement details for both structures are given in Table 2. The initial structural model for CTZ was taken from a 123 K single-crystal X-ray experiment (CCDC deposition code 666612) and refined against the PND data (six data banks),

[1] Supplementary data for this paper, including a detailed computational procedure, the results of the CSD search and complete CIF for all structures determined, are available from the IUCr electronic archives (BS5052). Services for accessing these data are described at the back of the journal.

Table 2
Crystal data for the title structures with simultaneous X-ray and neutron powder data refinement.

	CTZ_GEM_neutron_130K	HCT_GEM_neutron_295K
Crystal data		
Chemical formula	$C_7H_6ClN_3O_4S_2$	$C_7H_8ClN_3O_4S_2$
M_r	295.72	297.74
Cell setting, space group	Triclinic, $P\overline{1}$	Monoclinic, $P2_1/c$
Temperature (K)	130 (2)	295 (2)
a, b, c (Å)	4.8499 (3), 6.3694 (4), 8.9106 (6)	9.4855 (3), 8.3325 (2), 15.1201 (4)
α, β, γ (°)	74.401 (1), 83.865 (1), 80.524 (1)	90, 113.240 (3), 90
V (Å^3)	260.93 (3)	1098.08 (6)
Z	1	4
D_x (Mg m^{-3})	1.877	1.801
Radiation type	Neutron	Neutron
μ (mm^{-1})	0.12	0.04
Specimen form, colour	Cylinder (particle morphology: Needle), colourless	Cylinder (particle morphology: Needle), colourless
Specimen size (mm)	40 × 5	40 × 5
Specimen preparation temperature (K)	293	295
d-spacing range for refinement (Å)	1.10–6.30 (X-ray); 0.55–10.25 (neutron)	1.50–1.72 (X-ray); 0.99–10.25 (neutron)
Data collection		
Diffractometer	GEM, ISIS	GEM, ISIS
Data collection method	Specimen mounting: 5 mm vanadium cylindrical can; mode: transmission; scan method: time-of-flight	Specimen mounting: 5 mm vanadium cylindrical can; mode: transmission; scan method: time-of-flight
Absorption correction	Empirical (using intensity measurements)	Empirical (using intensity measurements)
Refinement		
Refinement on	Full profile	Full profile
R factors and goodness-of-fit	R_p = 0.04250, R_{wp} = 0.01104, R_{exp} = 0.00414, S = 2.62	R_p = 0.01660, R_{wp} = 0.00722, R_{exp} = 0.00259, S = 2.81
Wavelength of incident radiation (Å)	1.0985 (X-ray)	1.54056 (X-ray)
Excluded region(s)	Excluded short and long TOF regions†	Excluded short and long TOF regions‡
Profile function	Full Voigt with double exponential	Full Voigt with double exponential
No. of parameters	149	149
No. of restraints	6	24
H-atom treatment	Only coordinates refined	Only coordinates refined
Weighting scheme	Based on measured s.u.s, $w = 1/\sigma(Y_{obs})^2$	Based on measured s.u.s, $w = 1/\sigma(Y_{obs})^2$
$(\Delta/\sigma)_{max}$	0.001	0.001

Computer programs used: custom *ISIS* software; coordinates from single-crystal data; *TOPAS* (Coehlo, 2003). † < 1000.0 and > 8000.0 µs excluded 9° detector bank; < 1500.0 and > 15 000.0 µs excluded 18° detector bank; < 1800.0 and > 20 000.0 µs excluded 35° detector bank; < 2600.0 and > 20 200.0 µs excluded 64° detector bank; < 3700.0 and > 18 000.0 µs excluded 90° detector bank; < 5000.0 and > 16 600.0 µs excluded 153° detector bank. ‡ < 2000.0 and > 8000.0 µs excluded 9° detector bank; < 1900.0 and > 15 000.0 µs excluded 18° detector bank; < 2800.0 and > 20 000.0 µs excluded 35° detector bank; < 5000.0 and > 20 000.0 µs excluded 64° detector bank; < 9000.0 and > 18 000.0 µs excluded 90° detector bank; < 9000.0 and > 16 600.0 µs excluded 153° detector bank.

and the PXRD data (one data bank) in a simultaneous refinement using a restrained Rietveld method (Rietveld, 1969), as implemented in *TOPAS Academic* (Coelho, 2003, 2005). Soft distance restraints were applied to the six R—H bonds with the restraint distances set to the values as defined by Allen *et al.* (1987). Two common isotropic displacement factors were refined for non-H and H atoms, respectively. A similar refinement was carried out for HCT, with the initial structural model coming from a 123 K single-crystal X-ray re-determination (CCDC deposition code 666614). Soft distance restraints (Allen *et al.*, 1987) were employed on all bonded distances. The presence of a small amount (*ca* 8%) of HCT form I was modelled with a fixed structural model taken from a 123 K single-crystal X-ray re-determination (CCDC deposition code 666613). In both cases, soft restraints employed s.u. values of 0.01 Å. The overall penalties weighting factor (K1) within *TOPAS* was 1 for CTZ and 5 for HCT.

2.4. Software and other general procedures

The structures were analysed and visualized using the programs *MERCURY* (Bruno *et al.*, 2002) and *PLATON* (Spek, 2004).

3. Results and discussion

The crystal structures of the title compounds have been described elsewhere (Dupont & Dideberg, 1970, 1972; Shankland *et al.*, 1997; Florence, Johnston, Fernandes *et al.*, 2005).

The focus of our discussion lies in assessing the merits of joint refinement of PND and PXRD data for accurate structure determination of hydrogenous organic molecules. The results are summarized in Tables 3 and 4, and the supplementary data. Final Rietveld fits to the data for the case of CTZ are shown in Fig. 2. An equivalent figure for HCT can be found in the supplementary material.

At 26 and 32%, respectively, the H-atom content in CTZ and HCT is substantial and does indeed give rise to a large background in the PND data (see Fig. 2). Nevertheless, given sufficient data collection time, the coherent signal is clearly visible once the data have been reduced. The large d-spacing coverage of the GEM instrument, coupled with the lack of a form-factor fall-off for neutron scattering, means that the coherent signal is still visible at d spacings less than 1 Å. Indeed, it is possible to perform *completely unrestrained* refinements of both structures against their respective PND data and obtain structures where all component atoms are essentially correctly located. Nevertheless, it is important to remember that the PND are essentially medium resolution (Fig. 2*h*, $\Delta d/d \simeq 2 \times 10^{-3}$ for the GEM backscattering bank *cf.* $\Delta d/d \simeq 5 \times 10^{-4}$ for the backscattering bank of high-resolution powder diffractometer at ISIS) and so the extent of

Table 3
Comparison of bond lengths in CTZ determined from single-crystal X-ray diffraction at 123 K, from PXRD at 130 K and from the joint refinement of PXRD and PND data at 130 K.

Standard uncertainties for single-crystal data estimated from the variances of the full variance–covariance matrix; standard uncertainties for powder data calculated with *PLATON* (Spek, 2004).

Bond distance (Å)	Single-crystal X-ray	PXRD + PND restrained	PXRD restrained	PXRD + PND unrestrained
Cl1—C6	1.739 (3)	1.7064	1.7413	1.7025
S1—O1	1.429 (2)	1.441 (4)	1.439 (7)	1.443 (4)
S1—O2	1.433 (2)	1.429 (4)	1.464 (8)	1.425 (4)
S1—N1	1.619 (3)	1.619 (3)	1.664 (8)	1.628 (4)
S1—C3	1.742 (3)	1.737 (4)	1.769 (11)	1.745 (4)
S2—O3	1.431 (2)	1.431 (4)	1.406 (8)	1.417 (5)
S2—O4	1.434 (2)	1.446 (4)	1.479 (6)	1.446 (4)
S2—N3	1.607 (3)	1.576 (3)	1.578 (8)	1.587 (4)
S2—C5	1.772 (3)	1.737 (4)	1.775 (12)	1.753 (4)
N1—C1	1.299 (4)	1.316 (3)	1.283 (12)	1.319 (5)
N2—C1	1.341 (4)	1.377 (3)	1.230 (11)	1.392 (4)
N2—C2	1.393 (4)	1.371 (4)	1.392 (13)	1.377 (4)
N2—H2	0.86 (4)	0.995 (3)	0.98 (3)	0.920 (7)
N3—H3*A*	0.81 (4)	1.023 (4)	1.02 (4)	0.972 (6)
N3—H3*B*	0.81 (4)	0.994 (3)	1.03 (3)	1.048 (7)
C2—C3	1.397 (4)	1.429 (4)	1.416 (15)	1.425 (5)
C2—C7	1.400 (5)	1.422 (5)	1.392 (17)	1.425 (5)
C3—C4	1.393 (4)	1.399 (4)	1.402 (16)	1.415 (5)
C4—C5	1.383 (5)	1.398 (4)	1.371 (15)	1.412 (5)
C5—C6	1.408 (4)	1.417 (5)	1.403 (17)	1.407 (5)
C6—C7	1.368 (4)	1.360 (5)	1.374 (15)	1.354 (5)
C1—H1	0.9500	1.073 (3)	1.11 (4)	1.061 (8)
C4—H4	0.9500	1.067 (4)	1.06 (4)	1.011 (8)
C7—H7	0.9500	1.076 (4)	1.12 (3)	1.107 (9)

Table 4
Comparison of bond lengths in HCT determined from single-crystal X-ray diffraction at 123 K, from PXRD at 295 K, and from the joint refinement of PXRD and PND data at 295 K.

Standard uncertainties for single-crystal data estimated from the variances of the full variance–covariance matrix; standard uncertainties for powder data calculated with *PLATON* (Spek, 2004).

Bond distance (Å)	Single-crystal X-ray	PXRD + PND restrained	PXRD restrained	PXRD + PND unrestrained
Cl1—C7	1.7375 (17)	1.730 (2)	1.722 (4)	1.691 (7)
S1—O1	1.4310 (14)	1.439 (3)	1.432 (5)	1.467 (6)
S1—O2	1.4369 (14)	1.428 (3)	1.420 (5)	1.408 (6)
S1—N1	1.6398 (17)	1.6375 (16)	1.617 (4)	1.668 (5)
S1—C3	1.7554 (17)	1.759 (2)	1.753 (5)	1.725 (7)
S2—O3	1.4439 (13)	1.435 (3)	1.418 (5)	1.455 (7)
S2—O4	1.4360 (14)	1.428 (3)	1.418 (5)	1.425 (6)
S2—N3	1.6107 (17)	1.595 (2)	1.592 (5)	1.562 (5)
S2—C5	1.7647 (18)	1.759 (2)	1.738 (4)	1.767 (7)
N1—C1	1.470 (2)	1.460 (2)	1.456 (5)	1.438 (7)
N2—C1	1.449 (2)	1.463 (2)	1.449 (4)	1.464 (7)
N2—C2	1.365 (2)	1.410 (2)	1.390 (6)	1.360 (7)
N1—H5	0.79 (3)	1.003 (2)	1.00 (2)	0.964 (11)
N2—H2	0.82 (3)	1.005 (3)	1.00 (2)	0.975 (13)
N3—H3*A*	0.88 (3)	1.007 (3)	1.03 (2)	0.992 (10)
N3—H3*B*	0.82 (3)	1.005 (3)	1.01 (3)	1.027 (9)
C2—C3	1.416 (2)	1.394 (2)	1.380 (5)	1.438 (8)
C2—C7	1.410 (2)	1.390 (2)	1.374 (5)	1.438 (8)
C3—C4	1.387 (3)	1.382 (3)	1.369 (6)	1.377 (8)
C4—C5	1.390 (2)	1.389 (2)	1.374 (4)	1.484 (9)
C5—C6	1.409 (2)	1.387 (2)	1.371 (5)	1.374 (8)
C6—C7	1.373 (3)	1.381 (2)	1.366 (6)	1.386 (8)
C1—H1*A*	0.97 (2)	1.088 (2)	1.06 (3)	0.917 (12)
C1—H1*B*	0.97 (2)	1.089 (2)	1.07 (2)	1.130 (11)
C4—H4	0.95 (2)	1.083 (4)	1.06 (3)	0.998 (13)
C7—H7	0.95 (2)	1.080 (3)	1.07 (2)	0.970 (13)

reflection overlap, particularly at short d spacings, is substantial. As a consequence, the number of truly independent reflection intensities in the PND data is small and when the unrestrained structures are examined closely, many of the bond lengths and angles lie outside the range of expected values.

Similarly, whilst the PXRD data (*e.g.* Figs. 2*a* and *b*) clearly show the benefits of higher instrumental resolution, they suffer from X-ray form-factor fall-off at high 2θ and unrestrained refinements of CTZ and HCT again lead to heavily distorted (in terms of molecular geometry) backbone structures and very poorly determined H atoms.

Linking the two discrete data sources in a joint refinement gives the best features of both sources and unrestrained refinements are significantly better as a result (see Tables 3 and 4). Soft restraints were still employed (only R—H distances in the case of CTZ; all bond distances in the case of HCT, the data for the latter compound being of generally lower resolution to that obtained for CTZ) to 'tidy up' the final refinements, which are of high quality (Table 2). Note that the low R factors obtained are to some extent a function of the large background contribution from the incoherent scattering.

A comparison of the refinements of CTZ and HCT against the reference single-crystal X-ray structures (see Tables 3 and 4, and Fig. 3) shows good overall agreement, with the r.m.s. difference in the non-H atom positions being 0.026 and 0.092 Å for CTZ and HCT, respectively, and 0.030 and 0.101 Å for all atoms, respectively. The refinements show the expected lengthening of R—H bond lengths arising from the use of neutron data. In addition to this, significant improvements (an order of magnitude decrease) are seen in the precision of the H-atom positions in the unrestrained models, with consequent improvements in the precision of derived quantities involving those atoms. As expected, the s.u. values are on a par with those of the non-H atoms in the structures.

The potential for the orientation of SO_2NH_2 groups to be poorly determined (owing to the effectively equal X-ray scattering power of the substituents on the S atom) when structures are refined from PXRD data alone has been highlighted previously (Shankland & David, 2002). Having to rely upon assessment of the best crystal packing arrangement with respect to each of three possible orientations of the substituents is far from ideal. However, when neutron diffraction data are factored into a refinement, any ambiguities disappear, for two reasons:

(i) the difference in coherent neutron scattering lengths for oxygen (5.80 barns) and nitrogen (9.36 barns), and

(ii) the presence of the negatively scattering H atoms on the nitrogen.

Indeed, the impact of these two H atoms with respect to the fit to the PND and PXRD data, respectively, is easily assessed by simply deleting them from the thiazide input models and carrying out two Rietveld refinements. In the case of the PND-only refinements, the resultant structure is badly distorted in

the region of the SO_2NH_2 and the final R_{wp} is doubled with respect to the correct structure. In contrast, in the case of the PXRD-only refinement, the resultant structure is effectively unchanged and the R_{wp} was only marginally higher when compared with that of the correct structure.

The strategy presented in this work offers an experimental solution to the commonly encountered problem whereby X-ray diffraction data alone (single-crystal or powder) fail to provide a complete and accurate structural picture of phenomena related to H-atom positions, including:

(i) tautomerism – for example the tautomeric H atom in CTZ is clearly located on N2 (not N1, as is frequently shown in the chemical literature);

(ii) $-NH_2$ pyramidalization (CTZ and HCT are exemplars here);

(iii) hydrogen-bond geometry, including interactions with the solvent of crystallization, such as hydrates with missing or poorly determined water H atoms.

The actual PND experiment itself is completely straightforward – the experiment consists of no more than filling a

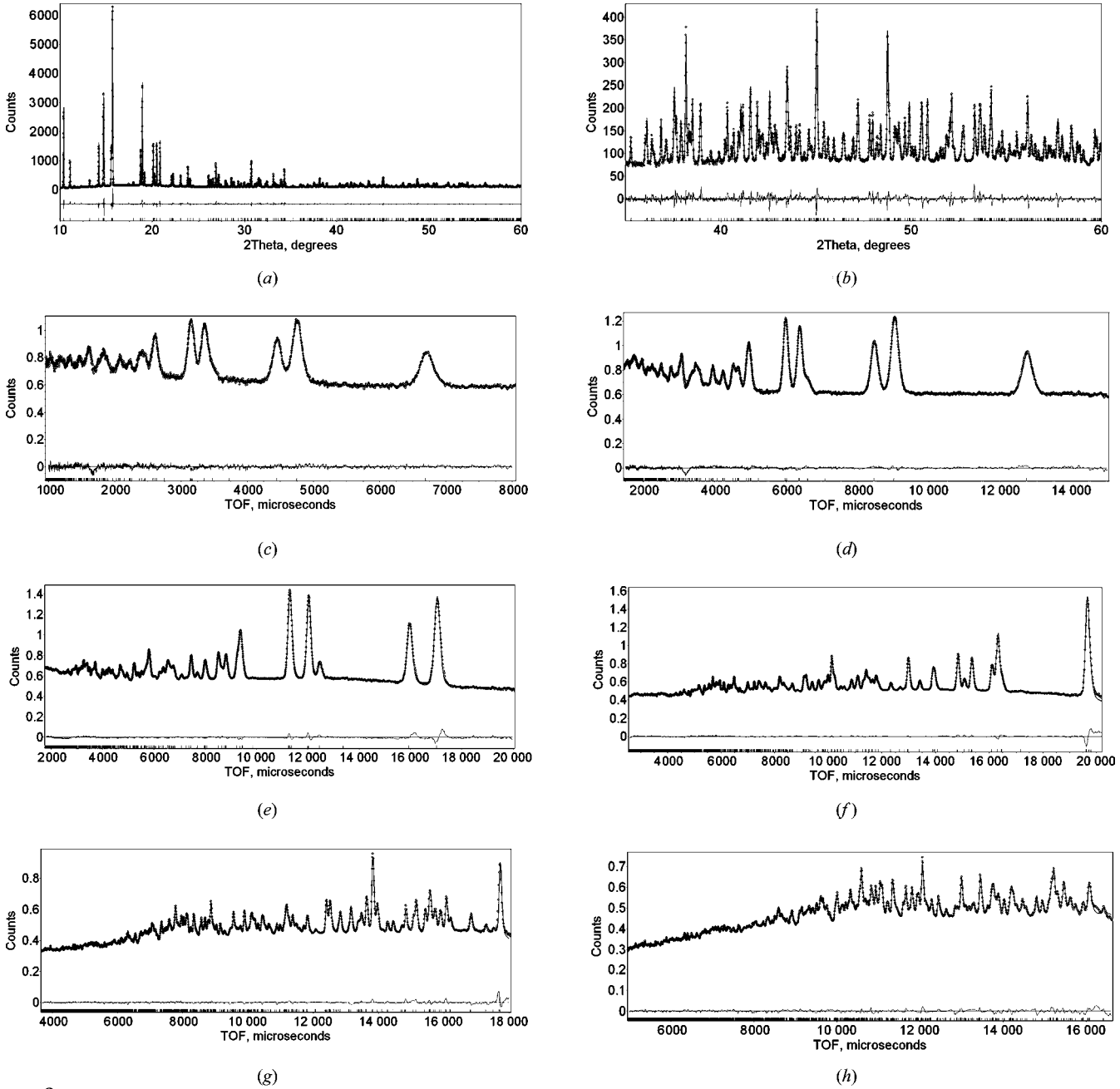

Figure 2
Rietveld profile fit for the (*a*), (*b*) PXRD and (*c*)–(*h*) PND data of CTZ. Observed data points are depicted as circles, calculated data points as a solid line, and the difference curve as a light grey line. The tick marks indicate reflection positions. For the neutron data: (*c*) detector bank 1 at $\sim 9^\circ$, (*d*) detector bank 2 at $\sim 18^\circ$, (*e*) detector bank 3 at $\sim 35^\circ$, (*f*) detector bank 4 at $\sim 64^\circ$, (*g*) detector bank 5 at $\sim 90^\circ$, (*h*) detector bank 6 at $\sim 135^\circ$. The *d*-spacing ranges shown (d_{min}–d_{max}) are: (*a*) 1.10–6.30 Å; (*c*) 1.28–10.25 Å; (*d*) 1.01–10.11 Å; (*e*) 0.64–7.14 Å; (*f*) 0.53–4.10 Å; (*g*) 0.54–2.70 Å; (*h*) 0.55–1.83 Å.

small vanadium can with the material under study, placing it in the sample position on the instrument, opening the instrument shutter, starting the data acquisition electronics, then stopping them ~ 8 h later. Clearly, a large volume of sample is needed (a consequence of the weak scattering of neutrons) and a significant amount of data-collection time is required to obtain a usable signal-to-background ratio. That said, neutron source powers are, in general, rising and instruments are continually under development. By way of example, we had previously collected PND data from CTZ on HRPD at ISIS and found that the data were of little value, as the overall count rates were too low to enable the coherent scattering to be seen against the incoherent background. However, HRPD is currently the subject of a supermirror-guide upgrade, which is expected to increase the incident flux by an order of magnitude across the board and by a factor of ~ 40 at short d spacings. This flux increase will enable materials such as CTZ to be studied more easily on HRPD, with all the consequent benefits of the extremely high instrumental resolution available, *e.g.* no soft restraints would be needed to 'tidy up' a joint refinement. As such, one may expect the role of PND in organic structure refinement to rise steadily from its current miniscule level.

4. Conclusions

The results presented here show that extremely valuable structural information can be obtained from polycrystalline molecular organic materials containing a large percentage of H atoms using PND. Key to the success of the structure refinements is the use of high count-rate, medium-resolution PND data taken in combination with high-resolution PXRD data; the combination of the two allows for accurate refinement of structural parameters with minimal resort to the use of restraints. It is likely that the supermirror guide upgrade to the HRPD instrument at ISIS will further extend the range of applicability of PND to this class of materials and greatly improve the results obtained from the use of the joint PND/PXRD Rietveld approach.

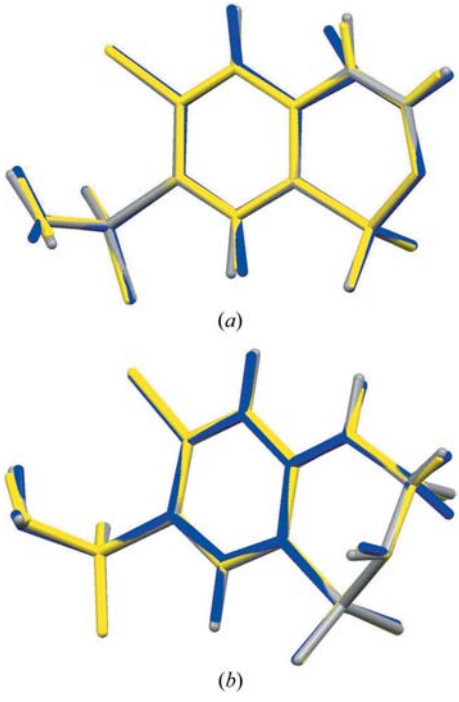

Figure 3
Structural overlays for (*a*) CTZ and (*b*) HCT. Colour scheme: grey = joint PXRD+PND (restrained); yellow = single-crystal X-ray; blue = PXRD (restrained).

The authors thank the Basic Technology Programme of the UK Research Councils for funding this work under the project Control and Prediction of the Organic Solid State (http://www.cposs.org.uk) and gratefully acknowledge the input received from Alan R. Kennedy (single-crystal data), Alastair J. Florence (PXRD data) and Norman Shankland (thiazide crystal structures).

References

Allen, F. H., Kennard, O., Watson, D. G., Brammer, L., Orpen, A. G. & Taylor, R. (1987). *J. Chem. Soc. Perkin Trans. II*, pp. S1–S18.
Bruno, I. J., Cole, J. C., Edgington, P. R., Kessler, M., Macrae, C. F., McCabe, P., Pearson, J. & Taylor, R. (2002). *Acta Cryst.* B**58**, 389–397.
Coelho, A. A. (2003). *J. Appl. Cryst.* **36**, 86–95.
Coelho, A. (2005). *TOPAS*, http://members.optusnet.com.au/alancoelho/.
Cruz Cabeza, A. J., Day, G. M., Motherwell, W. D. & Jones, W. (2006). *Cryst. Growth Des.* **6**, 1858–1866.
David, W. I. F., Shankland, K. & Ibberson, R. M. (2004). ISIS annual report, RAL-TR-2004–050, http://www.isis.rl.ac.uk/isis2004/highlights/David.htm.
Dupont, L. & Dideberg, O. (1970). *Acta Cryst.* B**26**, 1884–1885.
Dupont, L. & Dideberg, O. (1972). *Acta Cryst.* B**28**, 2340–2347.
Fernandes, P., Leech, C. K., Johnston, A., Shankland, K., David, W. I. F., Shankland, N. & Florence, A. J. (2007). *Acta Cryst.* E**63**, o3685.
Florence, A., Johnston, A., Fernandes, P., Shankland, K., Stevens, H. N. E., Osmundsen, S. & Mullen, A. B. (2005). *Acta Cryst.* E**61**, o2798–o2800.
Florence, A. J., Johnston, A. & Shankland, K. (2005). *Acta Cryst.* E**61**, o2974–o2977.
Hill, R. J. & Madsen, I. C. (2002). *Structure Determination from Powder Diffraction Data*, edited by W. I. F. David, K. Shankland, L. B. McCusker & Ch. Baerlocher, pp. 114–116. Oxford University Press.
Ibberson, R. M. (1996). *J. Mol. Struct.* **377**, 171–179.
Johnston, A., Florence, A. J., Fernandes, P. & Kennedy, A. R. (2007*a*). *Acta Cryst.* E**63**, o2423.
Johnston, A., Florence, A. J., Fernandes, P. & Kennedy, A. R. (2007*b*). *Acta Cryst.* E**63**, o2422.
Johnston, A., Florence, A. J., Shankland, N., Kennedy, A. R., Shankland, K. & Price, S. L. (2007). *Cryst. Growth Des.* **7**, 705–712.
Masciocchi, N., D'Alfonso, G., Kockelmann, W., Schafer, W. & Sironi, A. (1997). *Chem. Commun.* pp. 1903–1904.
Parkin, A., Seaton, C. C., Blagden, N. & Wilson, C. C. (2007). *Cryst. Growth Des.* **7**, 531–534.
Rietveld, H. M. (1969). *J. Appl. Cryst.* **2**, 65–71.
Shankland, K. & David, W. I. F. (2002). *Structure Determination from Powder Diffraction Data*, edited by W. I. F. David, K. Shankland,

L. B. McCusker & Ch. Baerlocher, pp. 280. Oxford University Press.
Shankland, K., David, W. I. F. & Silva, D. S. (1997). *J. Mater. Chem.* **7**, 569–572.
Spek, A. L. (2004). *PLATON*. Utrecht University, The Netherlands.
Weller, M. T., Henry, P. F. & Light, M. E. (2007). *Acta Cryst.* B**63**, 426–432.